CONDENSED MATTER PHYSICS

Subcycle dynamics of excitons under strong laser fields

Eduardo B. Molinero[1]*, Bruno Amorim[2], Mikhail Malakhov[3], Giovanni Cistaro[3], Álvaro Jiménez-Galán[1], Antonio Picón[3,4], Pablo San-José[1], Misha Ivanov[5,6,7,8], Rui E. F. Silva[1,5]*

Excitons play a key role in the linear optical response of two-dimensional (2D) materials. However, their role in the nonlinear response to intense, nonresonant, low-frequency light is often overlooked as strong fields are expected to tear the electron-hole pair apart. Using high-harmonic generation as a spectroscopic tool, we theoretically study their formation and role in the nonlinear optical response. We show that the excitonic contribution is prominent and that excitons remain stable even when the driving laser field surpasses the strength of the Coulomb field binding the electron-hole pair. We demonstrate a parallel between the behavior of strongly laser-driven excitons in 2D solids and strongly driven Rydberg states in atoms, including the mechanisms of their formation and stability. Last, we show how the excitonic contribution can be singled out by encapsulating the 2D material in a dielectric, tuning the excitonic energy and its contribution to the high-harmonic spectrum.

INTRODUCTION

When an electron is promoted from the valence to the conduction band, the attractive Coulomb interaction can bind together the electron and the hole left in the valence band into a quasiparticle, commonly known as excitons (*1*). In three-dimensional (3D) materials, their effect is often negligible due to the strong screening of the electronic interactions. However, this is not the case for 2D materials. In these systems, the reduced dimensionality enhances the interactions felt between electrons and holes. Thus, excitons have particularly substantial binding energies, have a substantial fraction of the gap, and play a dominant role in their linear optical response (*2*). Moreover, resonant one-photon excitation of excitonic states remains prominent even when a low-frequency field dresses the electron-hole pair (*3*). What should one expect for the highly nonlinear optical response when 2D solids interact with intense low-frequency laser fields?

This is a highly pertinent question for high-harmonic generation (HHG) in solids, which has emerged as an important direction in ultrafast condensed matter physics (*4*–*6*). Will excitons be formed when optical tunneling injects electrons in the conduction band? Will they survive the strong laser field, which exceeds the Coulomb field that binds the electron and the hole together? If yes, what will be the physics and the dynamics of their formation? How will the electron acceleration by the driving laser field away from the injection point affect this process?

Answering these questions is important both fundamentally and for applications. At the fundamental level, HHG offers a unique window into the electronic structure and dynamics in trivial, topological, and strongly correlated solids far from equilibrium (*7*–*28*). Interpreting these dynamics without understanding the role of excitons is hardly adequate. For applications, harnessing strong excitonic transitions during radiative electron-hole recombination would be important for HHG-based solid-state sources of bright ultrashort VUV-XUV (vacuum ultraviolet–extreme ultraviolet) radiation (*29*, *30*).

While the entry of intense light fields into condensed matter physics is relatively recent (*7*), light-matter interaction with such fields has been extensively studied in atoms (*31*). Rydberg states, the atomic analogs of excitons (*32*), were found to play an unexpectedly important role in strong-field ionization, the atomic analog of electron injection into the conduction band. Prominent examples are the so-called frustrated tunneling (*33*–*36*) and the Freeman resonances in multiphoton ionization (*36*, *37*). The remarkable stability of Rydberg states against intense laser fields, predicted in (*38*–*40*), was confirmed in (*41*, *42*), markedly demonstrated in (*35*), and even led to lasing during laser filamentation in dense gas (*43*). Multiphoton Rydberg excitations have been found to contribute to harmonic emission during the laser pulse (*44*–*46*) and free induction decay after its end (*47*, *48*). There have been beautiful works (*26*, *27*, *49*, *50*) on the effect of electronic interactions in solid-state HHG, e.g., showing that such interactions can enhance the total harmonic yield both theoretically (*50*) and experimentally (*51*). However, there has been a lack of an in-depth analysis of the dynamics and the physics of the creation and destruction of excitons in the strong field regime. Moreover, there have been experimental hints (*51*–*53*) that excitons do play a role in HHG in 2D materials. Their results motivate the need to understand the nonequilibrium dynamics of strongly driven excitons and the physics associated with their contributions to HHG in 2D materials.

Here, we aim to fill this gap by (i) unveiling that excitons not only display subcycle dynamics but also survive the laser field for many laser cycles, (ii) providing a clear physical equivalence between strongly driven excitons and Rydberg states in strong laser fields, and (iii) proposing a simple experimental setup to confirm the physics described here. We show that high-harmonic emission can reveal the formation of excitons by significantly increasing both the overall harmonic yield, by about an order of magnitude, and the emission intensity at energies near excitonic states, by about two orders of magnitude. We also show that shifting the exciton binding energy by using a substrate provides a telltale sign of their contributions. Time-resolved analysis of the emission shows the formation dynamics and the

[1]Instituto de Ciencia de Materiales de Madrid (ICMM), Consejo Superior de Investigaciones Científicas (CSIC), Sor Juana Inés de la Cruz 3, 28049 Madrid, Spain. [2]Centro de Física das Universidades do Minho e do Porto (CF-UM-UP) and Laboratory of Physics for Materials and Emergent Technologies (LaPMET), Universidade do Minho, 4710-057 Braga, Portugal. [3]Departamento de Química, Universidad Autónoma de Madrid, 28049 Madrid, Spain. [4]Condensed Matter Physics Center (IFIMAC), Universidad Autónoma de Madrid, 28049 Madrid, Spain. [5]Max Born Institute, Max-Born-Straße 2A, 12489 Berlin, Germany. [6]Department of Physics, Humboldt University, Newtonstraße 15, 12489 Berlin, Germany. [7]Blackett Laboratory, Imperial College London, London SW7 2AZ, UK. [8]Technion–Israel Institute of Technology, 3200003 Haifa, Israel.
*Corresponding author. Email: ebmolinero@gmail.com, e.b.molinero@csic.es (E.B.M.); ruiefdasilva@gmail.com, rui.silva@csic.es (R.E.F.S.)

remarkable stability of excitons against strong light fields. In spite of the emergent, many-body nature of excitons, we consistently find strong similarity in their strong field dynamics with that of single-particle Rydberg states. This connection highlights how a nontrivial emergent quasiparticle, such as an exciton in a sea of interacting electrons, can behave much like a single-particle excitation in an atomic gas, even when driven by an intense field.

RESULTS

The nonlinear optical response of excitons in 2D materials can be simulated using real-time equations of motion (see Methods). We perform simulations on monolayer hexagonal boron-nitride (hBN). The choice of material has several motivations: It is a prototypical 2D insulator (*54*) and it hosts excitonic states with large binding energies (*55*, *56*). Furthermore, one can engineer the interactions by changing the substrate: A substrate with a higher dielectric constant effectively screens electronic interactions, reduces the electron-hole binding energy (*57*, *58*), and shifts the first excitonic state closer to the conduction band. This behavior is illustrated in Fig. 1B, which shows the absorption spectrum (see Methods for further information) by comparing the optical response of freestanding hBN and hBN in the presence of a SiO_2 substrate.

We have considered a laser pulse in the mid-infrared regime (3 μm) with an intensity of 1.16 TW/cm^2, a total duration of 20 optical cycles and with a cos^2 envelope. We show results for the field oriented along the $\Gamma - K$ direction. We have checked that the intensity is high enough to produce a nonlinear response of the material while being away from the material damage threshold. Moreover, we have ensured that the density of photoexcited carriers is far away from the exciton Mott threshold (*59*). However, we note that the effects are robust against variations of the parameters.

As a first step, we have performed two calculations: one where the excitons are present and another where the excitonic effects are neglected. In Fig. 2 (A and B), we show the comparison of the high-harmonic spectrum between the system with and without the excitons. In both cases, they display the general trend of HHG in solids, i.e., the amplitude of low-order harmonics decays as the order is increased, until the energy of the harmonics equals the bandgap of the material, here roughly at the 10th harmonic. At this point, a plateau of high-harmonics emerges, but once they reach their cutoff condition (around the 30th harmonic), an exponential decay of the harmonics ensues (*4*, *60*). Although the qualitative behavior in the two calculations is similar, there is also a major difference between the interacting and noninteracting scenarios: In the presence of excitons, we find strong enhancement in the intensity between the 5th and the 11th harmonic (gray areas in Fig. 2). This two orders of magnitude enhancement correlates with the energy of excitons in hBN. Another visible difference is the enhancement of harmonics in the plateau region by about an order of magnitude.

Excitons are bound states with energies inside the gap of the single-particle spectrum, situated between the valence and conduction bands. Qualitatively, one can say that they offer additional channels for electron injection across the bandgap in the presence of a strong laser field: Excitons act as "stepping stones" for electron injection across the gap. This explains the overall enhancement of harmonics in the

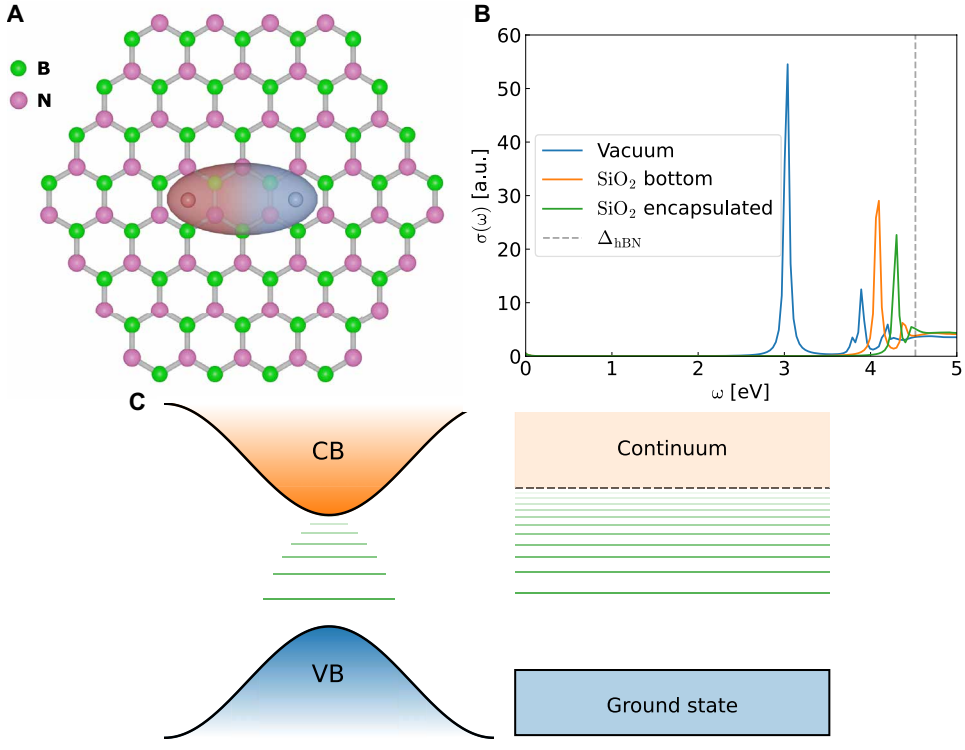

Fig. 1. Schematic diagrams. (**A**) Crystalline structure of hBN alongside a depiction of an exciton. (**B**) Real part of the optical conductivity, denoted by σ(ω), of monolayer hBN for different substrates. a.u., arbitrary units. (**C**) Schematic diagram to clarify the equivalence between the two systems: an exciton and an atomic Rydberg state. VB, valence band; CB, conduction band.

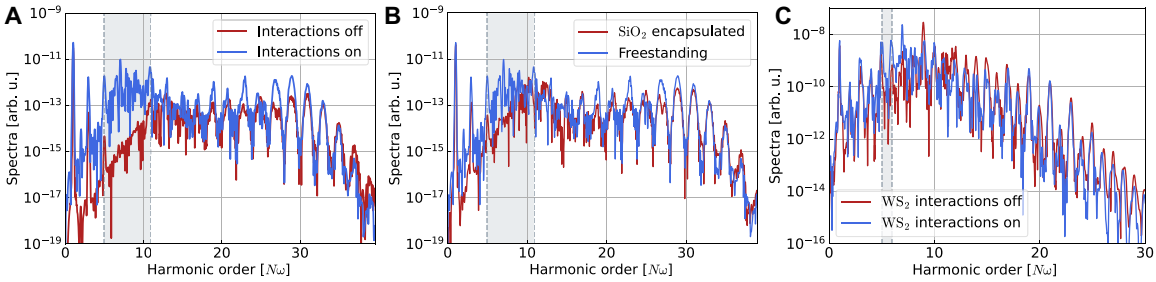

Fig. 2. High-harmonic spectra for hBN and WS_2. (**A**) HHG spectrum computed for a monolayer of hBN with (blue color) and without (red color) electronic interactions. arb. u., arbitrary units. (**B**) HHG spectrum computed for a monolayer of freestanding hBN (blue) and encapsulated in SiO_2 (red). The spectrum is obtained for a laser pulse in the $\Gamma - K$ direction and is shown for the component along the parallel direction. (**C**) Total spectrum calculated for a monolayer of WS_2 with and without interactions.

plateau region when including the excitons. Moreover, the biggest amplification is concentrated near the fifth/seventh harmonic, which corresponds to an energy of 2.1/2.9 eV. This energy region is close to the difference $\Delta_{\text{hBN}} - E_{\text{bind}}$ between the hBN bandgap $\Delta = 4.52$ eV and the binding energy of the exciton $E_{\text{bind}} \approx 1.5$ eV (*55*, *61*–*64*). In other words, the HHG enhancement produced by the excitonic states occurs around the energy required for a valence-band electron to transition into the first exciton state. We have checked that reducing the wavelength of the driving field leads to an increase in the yield efficiency because we are approaching the multiphoton regime (see Methods).

Moreover, the effect here described is general to 2D insulators/semiconductors and is not unique to hBN. This is exemplified in Fig. 2C, where we show the high-harmonic spectrum of WS_2 (see Methods) with and without interactions. There, one can appreciate that, when we include interactions, an enhancement in the harmonic yield emerges at the energetic region of the excitonic states. In this case of WS_2, this happens between the fifth and the sixth harmonic; the energy of the first exciton is $E_1 \approx 1.98$ eV (*65*), which corresponds to the fifth harmonic, while the gap $\Delta_{\text{WS2}} = 2.31$ eV corresponds to the sixth harmonic. The narrowing of the enhancement region happens because the excitonic states in WS_2 are very close to the optical gap. Thus, the harmonic spectra reflect how excitons open new pathways for electron injection in the interacting case. Furthermore, a comparison with the results obtained in time-dependent density functional theory (using local exchange-correlation potentials) simulations, where it was found that the inclusion of electronic interactions did not significantly affect the overall harmonic spectra (*12*, *66*), validates this picture: It is not electronic interactions per se that that cause the enhancement in the harmonic yield but rather the presence of excitonic states within the nonequilibrium dynamics. The real-time bonding of the electron and the hole can only be correctly captured if one takes into account long-range correlations (*67*).

Although comparing interacting and noninteracting systems may seem relevant on its own, it is not possible to switch interactions on and off in a laboratory experiment. However, electronic interactions can be screened by encapsulating the system in a dielectric material. In Fig. 2B, we compare the high-harmonic spectra for a freestanding hBN versus hBN encapsulated in silica, which acts as a strong dielectric. We see that the same physics takes place: Harmonic intensities are enhanced when the electron interactions are stronger. However, incomplete screening of the interaction makes the effect less pronounced that in Fig. 2A (red curve), where the interactions were completely turned off. This clearly demonstrates persistence of certain excitonic states (see Fig. 1B). The tunability of excitons in 2D materials, facilitated by the substrate, offers an experimental platform for investigating the behavior of these quasiparticles in strong laser fields, with HHG as an all-optical signature.

We have seen that excitons have a strong influence on the highly nonlinear optical response. However, should we expect that excitons both are formed and survive after the end of the strong laser pulse? What is the dynamics of their formation? To answer these questions, we have computed the Gabor transform of the generated current, both during and after the laser pulse. Figure 3 (A and B) shows the time-resolved harmonic emission for the noninteracting and interacting systems. One can clearly see a relevant enhancement in the emission below the bandgap (black line) due to the presence of extra channels. An intriguing feature observed in the Gabor profile is the appearance of a more complicated interference pattern when excitons are present in the system. Moreover, clear signatures of exciton survival after the pulse can be observed. In the presence of interactions, coherent emission occurs precisely at the binding energy of the exciton as the field ramps down. A clear enhancement in the emission near the excitonic energy during the ramp-down on the laser pulse as well as the persistence of radiation at the excitonic energy (red dashed line) after the end of the laser pulse demonstrate that excitons are most likely to both form and survive the strong laser field as the field is ramped down. To verify this, we have performed a Gabor transform with a reduced width, thereby increasing the resolution in the frequency domain (see Fig. 4, C and D). Strong pulses not only create excitons but also stabilize them, just as happens with Rydberg states in atoms driven by low-frequency laser fields, with the formation mechanism known as frustrated tunneling [see, e.g., (*35*, *36*)]. All our observations, including the formation of excitons at both the leading and the trailing edge of the driving laser pulse, with the survival most likely after formation at the trailing edge, are consistent with a solid-state analog of frustrated tunneling in atomic systems. Furthermore, one can see in Fig. 3B that the harmonic yield in the excitonic region goes from a peak to a valley within one cycle of the laser field, indicating the existence of subcycle dynamics of excitons. Such a behavior can be better appreciated in Fig. 3C, where we show the integrated Gabor profile around the first excitonic energy. We can observe that the harmonic signal at these energies becomes appreciable at around 70 fs, when the field is increasing, a clear footprint of the exciton formation. Also, the maximum harmonic emission around the excitonic energy occurs at around 150 fs, when the field is ramping down. As in the formation of Rydberg states in atoms, we have two events in the pulse where excitons are formed. After the

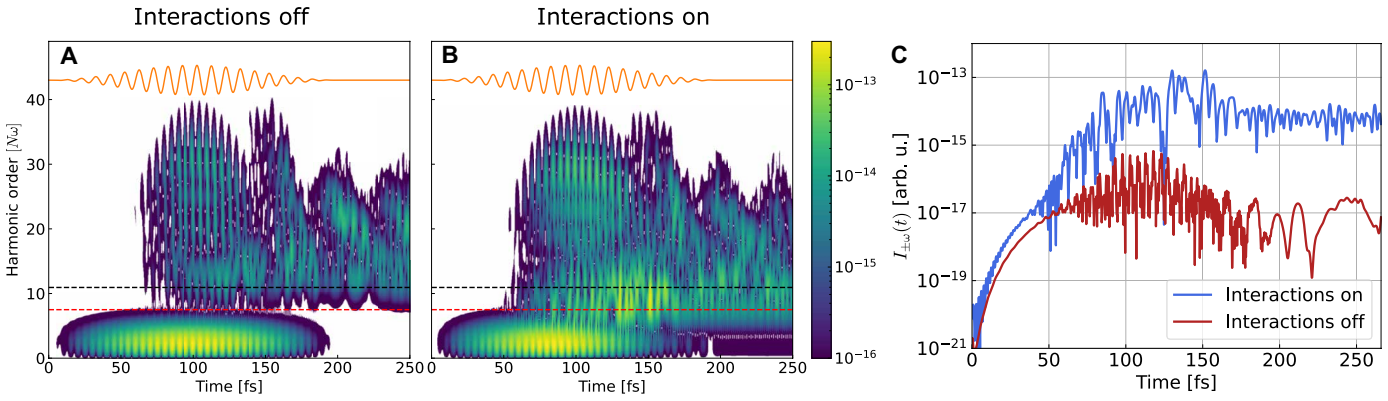

Fig. 3. Gabor profile of the harmonic signal. (**A**) Non-interacting case. (**B**) Interacting case. In both cases, the Gabor transform has a Gaussian window with the width $\sigma = (2\omega_L)^{-1}$, where ω_L is the laser frequency. The two horizontal dashed lines correspond to the energies associated with Δ_{hBN} (black) and E_{bind} (red), while the orange line depicts the electric field. (**C**) Integrated Gabor profile (see Methods) around the first exciton energy with and without interactions.

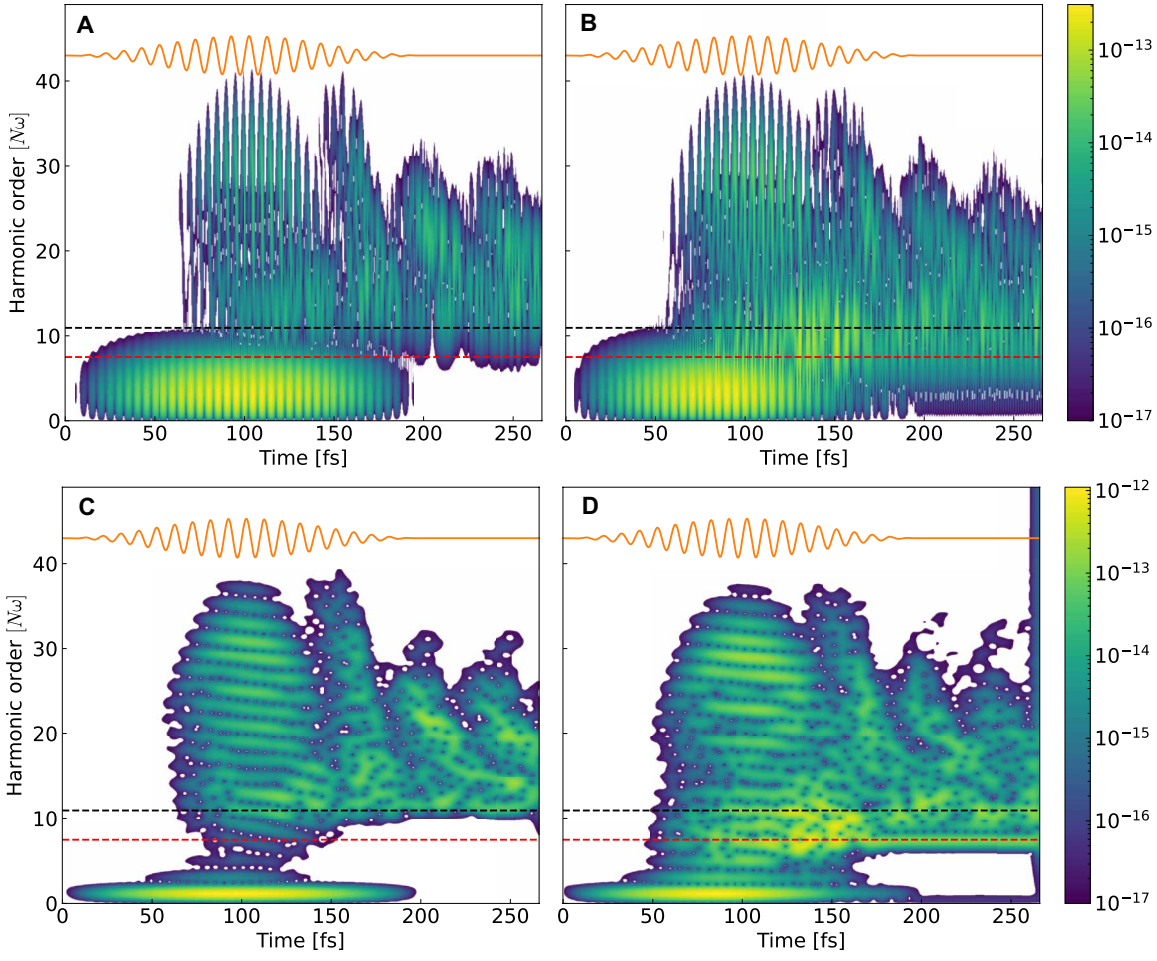

Fig. 4. Gabor profile of the harmonic signal for different widths. The first column corresponds to the noninteracting case, while the second one corresponds to the interacting case. (**A** and **B**) A window of $\sigma = (3\omega_L)^{-1}$. (**C** and **D**) A window of $\sigma = (\omega_L/2)^{-1}$. The two horizontal dashed lines correspond to the energies associated with Δ_{hBN} (black) and E_{bind} (red), while the orange line depicts the electric field.

end of the pulse, free induction decay from the exciton can be observed, a clear signal that excitons are not only formed but also stabilized by the strong laser field. These results allow us to answer the questions formulated earlier in the manuscript: first, that excitons unequivocally survive the laser field for many laser cycles and, second, that strongly driven excitons display subcycle (near the femtosecond scale) dynamics.

To investigate this atomic analogy further, we note that, within a first approximation, excitons are solutions to the Wannier equation (*68*), which is nothing but a single-particle Schrödinger equation for a centrosymmetric potential. This observation suggests that the HHG spectrum of an interacting insulator could be approximately described using a simple, noninteracting atomic model, where excitons are replaced by excited states of the atom. How far does this analogy go in the presence of a strong laser field? Can the whole system be qualitatively described using an atomic model?

To answer this question, we use a 1D atomic model (see Methods for more details) that intends to capture the physics of hBN excitons. The key idea is to use of a soft-core potential

$$V_{\alpha,\beta}(x) = \frac{\alpha}{\sqrt{x^2 + \beta^2}} \quad (1)$$

and adjust its parameters, α and β, so that the energy difference between the ground and the first excited state matches the crucial energy scale $\Delta_{hBN} - E_{bind}$. More specifically, we fix the ground state energy to $E_0 = -\Delta_{hBN}$ and the first excited state to $E_1 = -E_{bind}$ (see the diagram in Fig. 5A). The laser pulse parameters are the same as in the hBN case, except for an increased laser intensity of 4.5 TW/cm^2; this particular value was chosen so that the cutoff in the harmonics is the same in both systems. Figure 5B shows the HHG spectrum of the atomic model in terms for various E_1 energies. The spectrum displays the typical characteristics of an atomic spectrum (*31*): the low-order, perturbative harmonics, followed by the plateau harmonics caused by the recombination processes. It is worth noting that, when the energy of the first excited state E_1 is raised, the appearance of the plateau shifts to higher harmonic frequencies. Such a shift can be understood in the same way as for the hBN case: The closer the first excited is to the ground state, the more likely it is to help the electron to transition into the continuum, thus facilitating the onset of the plateau in the harmonic spectrum. This is also the kind of enhancement produced by Rydberg states found in atomic gases (*45*).

To better understand the similarities between the two systems, we conducted a scan encompassing different excitonic energies. Although the exciton binding energy E_{bind} is, in principle, a fixed physical quantity (at least if one neglects screening effects from the electrostatic environment), we can adjust its value from 2.0 to 0.1 to clarify its effect on the HHG spectrum. This is done by changing the amplitude of the Rytova-Keldysh potential (*62*). For each binding energy, we then compute the corresponding parameters α and β of $V_{\alpha,\beta}(x)$. In Fig. 6A, we plot the result, comparing the HHG spectrum between the 2D system and the atomic one in terms of the first exciton binding energies. Both systems display a qualitatively similar HHG spectrum; the enhancement is located precisely at the specific harmonic that corresponds to $\Delta_{hBN} - E_{bind}$ (see the dashed line). The similarity between Fig. 6A and Fig. 6B is notable given that these correspond to two very different physical problems: one describes the nonlinear electron dynamics of a 2D material with electron-electron interaction while the other corresponds to a 1D noninteracting atom. The common denominator between the two systems is, as mentioned before, the existence of a ground state separated from a continuum of states by a range of excited states between those two (see Fig. 6B), even if their nature (two-particle versus single-particle) is completely different. There are other obvious differences, such as the existence of dispersive bands above the gap in the 2D crystal. However, the qualitative aspects of electron dynamics are similar in spite of these differences. Fundamentally, the key quantity that controls the rate of transition (*4*, *31*), and hence the emission intensity, is the energy of the lowest excitation $\Delta_{hBN} - E_{bind} = |E_0| - |E_1|$. In this context, therefore, an interacting 2D crystal can be understood qualitatively using a noninteracting atomic gas model, where excitons play the same role as Rydberg states in enhancing the HHG response (*45*, *56*).

DISCUSSION

Our results show a significant increase in the high-harmonic emission when accounting for many-body interactions in 2D materials. The enhancement is clearly attributed to the population of excitonic states. Specifically, the enhancement is located at the energy difference between the valence band and the first excitonic state; the excitons act as extra channels for electron injection from the valence to the conduction band. Furthermore, we showed that this phenomenon is general to gapped 2D materials as it takes place for both insulators (e.g., hBN) and semiconductors (e.g., WS_2). An effective test of the

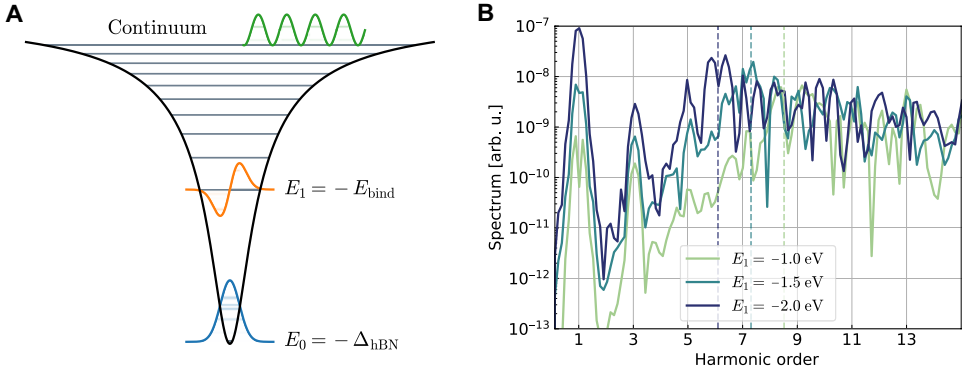

Fig. 5. Details of the atomic model. (**A**) Schematic diagram of $V_{\alpha,\beta}(x)$. (**B**) High-harmonic spectrum for the atomic model for different energies of the first excited state. Dashed lines denote the place where the difference $|E_0| - |E_1|$ lies for each E_1.

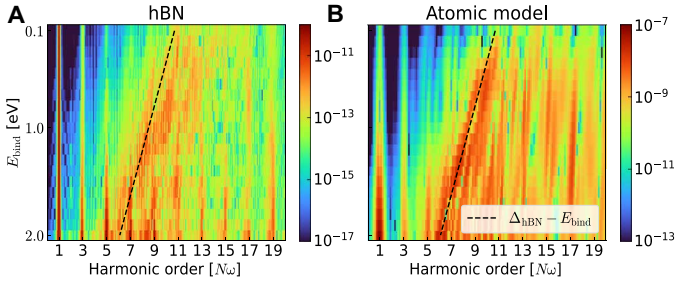

Fig. 6. Comparison between excitons in solid-state systems and an atomic system. High-harmonic spectrum comparison between the hBN system (**A**) and the atomic case (**B**). The black dashed lines denote where the line $\Delta_{\text{hBN}} - E_{\text{bind}}$ lies.

effect of excitons in strong field response can be performed by encapsulating a 2D material inside a stronger dielectric, thus tuning the exciton energy. We have found that excitons do survive such strong pulses, in analogy with Rydberg states in atoms. Last, comparing a simple atomic model with the solid-state simulations shows the same qualitative physics in both systems: The presence of excited states between a fixed ground state and a continuum leads to an enhancement in high-harmonic spectra. Our work suggests that a rich variety of phenomena emerging in atomic physics and associated with the formation of Rydberg states in strong laser fields, such as Freeman's resonances, frustrated tunneling, stabilization against ionization, and others, can be explored and exploited in 2D solids.

METHODS

SBE simulations

The microscopic response of the system to the laser field was obtained by numerically solving the semiconductor Bloch equations (SBEs) in the Wannier gauge (*62*, *69*). These equations, in atomic units (au), read

$$i\partial_t \rho_{nm}(\mathbf{k}, t) = \left[H^{(0)}(\mathbf{k}) + \Sigma(\mathbf{k}, t), \rho(\mathbf{k}, t)\right]_{nm} \quad (2)$$

$$+ \mathbf{E}(t) \cdot \left[\mathbf{A}(\mathbf{k}), \rho(\mathbf{k}, t)\right]_{nm} \quad (3)$$

$$+ i\mathbf{E}(t) \cdot \nabla_{\mathbf{k}} \rho_{nm}(\mathbf{k}, t) \quad (4)$$

where $H^{(0)}_{nm}(\mathbf{k})$ are the noninteracting terms of the Hamiltonian, $\Sigma_{nm}(\mathbf{k}, t)$ accounts for the electronic Coulomb interactions, $\mathbf{A}_{nm}(\mathbf{k})$ are the multiband Berry connection terms, and n and m refer to the band indexes. The electronic interaction are incorporated in the dynamics at the Fock level (*61*, *62*). More formally, this means that the self-energy is calculated using

$$\Sigma_{nm}(\mathbf{k}, t) = -\sum_{\mathbf{k}'} V_{nm}(\mathbf{k} - \mathbf{k}')\left[\rho_{nm}(\mathbf{k}', t) - \rho^0_{nm}\right]$$

where the initial state, $\rho^0_{nm} = \rho_{nm}(\mathbf{k}, 0)$, is completely filled for all the states below the Fermi energy. The subtraction $\rho_{nm}(\mathbf{k}', t) - \rho^0_{nm}$ is done to ensure that we not take into account interactions in the equilibrium state.

The potential, $V_{nm}(\mathbf{k} - \mathbf{k}')$, reads

$$V_{nm}(\mathbf{k} - \mathbf{k}') = \sum_{\mathbf{G}} e^{i(\mathbf{k} - \mathbf{k}' + \mathbf{G}) \cdot (\tau_n - \tau_m)} V(\mathbf{k} - \mathbf{k}' + \mathbf{G})$$

where τ_n are the center of the Wannier orbitals and $\mathbf{G}$ are the vectors of the reciprocal lattice. The sum over $\mathbf{G}$ is done to ensure the periodicity of the system. Here, $V(\mathbf{q})$, is the Fourier transform of the Rytova-Keldysh potential, which is known to accurately capture screening and dielectric effects in 2D materials (*70*, *71*).

For the monolayer hBN, we used the tight-binding model in which only the p_z orbitals are considered (*62*, *69*, *72*). The hopping parameter, t_0, was set to −2.8 eV and the onsite energy for the two atomic species was set to $\varepsilon_{B/N} = \pm$ 2.26 eV. The density matrix was constructed in a 300 × 300 Monkhorst-Pack grid, and it was time-propagated using a fourth-order Runge-Kutta with a timestep of $dt = 0.1$ au. Convergence was ensured for all the numerical parameters. To obtain the band structure and the dipole coupling elements of WS_2, we performed ab initio calculations using the Quantum Espresso code (*73*). We used a Heyd-Scuseria-Ernzerhof exchange-correlation hybrid functional on a Monkhorst-Pack grid of 12 × 12 × 4 points without spin-orbit coupling. We then projected the band structure onto a set of maximally localized Wannier functions using the wannier90 code (*74*). More precisely, the Bloch wave functions were then projected onto the d orbitals of tungsten to obtain the Wannier functions. The following projection results in a five-band model with one valence band and four conduction bands. We parametrized the Rytova-Keldysh potential following ref. (*65*).

Gabor analysis

The Gabor profile of a current $J(t)$ is formally defined as

$$\mathcal{G}_J(\omega, t) = \frac{2}{3\pi c^3} \int_0^{t_f} d\tau J(\tau) e^{i\omega\tau} e^{-\frac{(t-\tau)^2}{\sigma}} \quad (5)$$

where t_f is the total duration of the pulse and σ is the width of the Gaussian envelope. Hence, the Gabor transform can be viewed as a time-resolved Fourier transform. The resolution in either the frequency or time domain is determined by the magnitude of σ. Increasing σ results in better time domain resolution, while decreasing it leads to improved frequency domain resolution. Such a behavior can be appreciated in Fig. 4.

The integrated power spectrum shown in Fig. 3 is defined as

$$I_{\pm E}(t) = \int_{E-\Delta\omega}^{E+\Delta\omega} \mathcal{G}_J(\omega, t) d\omega \quad (6)$$

where E is the chosen energy (in our case, the binding energy of the first exciton) and Δω is the size of the integration interval. We have checked that the behavior of $I_{\pm E}(t)$ is robust under the variations on Δω.

Wavelength dependence

We have conducted a scan over the driving wavelength, from 3 to 2 μm, to check the spectral efficiency of the process. The results are shown in Fig. 7, where one can see that, as we reduce the wavelength and we approach the resonant regime, the spectral efficiency increases. This is particularly clear for the case of 2 μm, which corresponds to a photon energy of $\omega_2 = 0.62$ eV. For that photon energy, reaching the first excitonic state corresponds to $E_1/\omega_2 \sim 5$, i.e., reaching the exciton is a five-photon process, which results in the increased yield for that harmonic when we reduce the wavelength of the driving field, as one would expect.

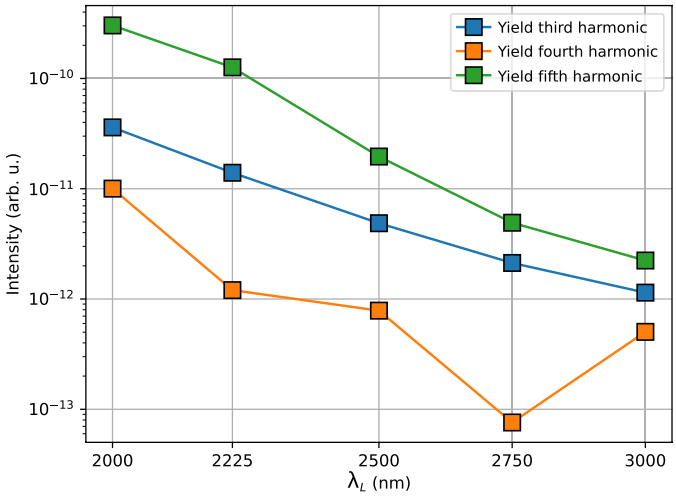

Fig. 7. Wavelength dependence. Yield of the third, fourth, and fifth harmonic in terms of the wavelength, λ_L, of the driving field.

Atomic model

The atomic model is based on the solution of the time-dependent Schrödinger equation (TDSE) for a 1D atom in the presence of a strong laser field. In atomic units, the TDSE reads

$$i\partial_t \Psi(x,t) = \left[T_{\text{kin}} + V_{\alpha,\beta}(x) + E(t)\cdot x\right]\Psi(x,t) \qquad (7)$$

where T_{kin} is the electronic kinetic energy, $V_{\alpha,\beta}(x)$ is the soft-core potential (Eq. 1 and Fig. 5A), and $E(t)$ is the electric field. The TDSE was solved numerically using a fourth-order Runge-Kutta method with a timestep of $dt = 0.1$ au. The initial state, $\Psi(x,0)$, was selected as the ground state of the time-independent Hamiltonian $H = T_{\text{kin}} + V_{\alpha,\beta}$. The calculations were performed in a box of length $L = 1000$ au with a grid spacing of $dx = 0.25$ au. We checked that convergence was achieved for all numerical parameters. The obtained HHG spectra obtained for this model can be appreciated in Fig. 5B.

REFERENCES AND NOTES

1. S. W. Koch, M. Kira, G. Khitrova, H. M. Gibbs, Semiconductor excitons in new light. *Nat. Mater.* **5**, 523–531 (2006).
2. G. Wang, A. Chernikov, M. M. Glazov, T. F. Heinz, X. Marie, T. Amand, B. Urbaszek, *Colloquium*: Excitons in atomically thin transition metal dichalcogenides. *Rev. Mod. Phys.* **90**, 021001 (2018).
3. S. V. B. Jensen, L. B. Madsen, A. Rubio, N. Tancogne-Dejean, High-harmonic spectroscopy of strongly bound excitons in solids. *Phys. Rev. A* **109**, 063104 (2024).
4. S. Y. Kruchinin, F. Krausz, V. S. Yakovlev, *Colloquium*: Strong-field phenomena in periodic systems. *Rev. Mod. Phys.* **90**, 021002 (2018).
5. S. Ghimire, D. A. Reis, High-harmonic generation from solids. *Nat. Phys.* **15**, 10–16 (2019).
6. E. Goulielmakis, T. Brabec, High harmonic generation in condensed matter. *Nat. Photonics* **16**, 411–421 (2022).
7. S. Ghimire, A. D. DiChiara, E. Sistrunk, P. Agostini, L. F. DiMauro, D. A. Reis, Observation of high-order harmonic generation in a bulk crystal. *Nat. Phys.* **7**, 138–141 (2010).
8. G. Vampa, T. J. Hammond, N. Thiré, B. E. Schmidt, F. Légaré, C. R. McDonald, T. Brabec, P. B. Corkum, Linking high harmonics from gases and solids. *Nature* **522**, 462–464 (2015).
9. T. T. Luu, M. Garg, S. Y. Kruchinin, A. Moulet, M. T. Hassan, E. Goulielmakis, Extreme ultraviolet high-harmonic spectroscopy of solids. *Nature* **521**, 498–502 (2015).
10. P. G. Hawkins, M. Y. Ivanov, V. S. Yakovlev, Effect of multiple conduction bands on high-harmonic emission from dielectrics. *Phys. Rev. A* **91**, 013405 (2015).
11. M. S. Wismer, S. Y. Kruchinin, M. Ciappina, M. I. Stockman, V. S. Yakovlev, Strong field resonant dynamics in semiconductors. *Phys. Rev. Lett.* **116**, 197401 (2016).
12. N. Tancogne-Dejean, O. D. Mücke, F. X. Kärtner, A. Rubio, Impact of the electronic band structure in high-harmonic generation spectra of solids. *Phys. Rev. Lett.* **118**, 087403 (2017).
13. N. Tancogne-Dejean, M. A. Sentef, A. Rubio, Ultrafast modification of Hubbard *U* in a strongly correlated material: Ab initio high-harmonic generation in NiO. *Phys. Rev. Lett.* **121**, 097402 (2018).
14. Y. Murakami, M. Eckstein, P. Werner, High-harmonic generation in Mott insulators. *Phys. Rev. Lett.* **121**, 057405 (2018).
15. R. E. F. Silva, I. V. Blinov, A. N. Rubtsov, O. Smirnova, M. Ivanov, High-harmonic spectroscopy of ultrafast many-body dynamics in strongly correlated systems. *Nat. Photonics* **12**, 266–270 (2018).
16. R. E. F. Silva, Á. Jiménez-Galán, B. Amorim, O. Smirnova, M. Ivanov, Topological strong-field physics on sub-laser-cycle timescale. *Nat. Photonics* **13**, 849–854 (2019).
17. A. Chacón, D. Kim, W. Zhu, S. P. Kelly, A. Dauphin, E. Pisanty, A. S. Maxwell, A. Picón, M. F. Ciappina, D. E. Kim, C. Ticknor, A. Saxena, M. Lewenstein, Circular dichroism in higher-order harmonic generation: Heralding topological phases and transitions in Chern insulators. *Phys. Rev. B* **102**, 134115 (2020).
18. A. J. Uzan, G. Orenstein, Á. Jiménez-Galán, C. McDonald, R. E. F. Silva, B. D. Bruner, N. D. Klimkin, V. Blanchet, T. Arusi-Parpar, M. Krüger, A. N. Rubtsov, O. Smirnova, M. Ivanov, B. Yan, T. Brabec, N. Dudovich, Attosecond spectral singularities in solid-state high-harmonic generation. *Nat. Photonics* **14**, 183–187 (2020).
19. C. Orthodoxou, A. Zaïr, G. H. Booth, High harmonic generation in two-dimensional Mott insulators. *NPJ Quantum Mater.* **6**, 76 (2021).
20. C. P. Schmid, L. Weigl, P. Grössing, V. Junk, C. Gorini, S. Schlauderer, S. Ito, M. Meierhofer, N. Hofmann, D. Afanasiev, J. Crewse, K. A. Kokh, O. E. Tereshchenko, J. Güdde, F. Evers, J. Wilhelm, K. Richter, U. Höfer, R. Huber, Tunable non-integer high-harmonic generation in a topological insulator. *Nature* **593**, 385–390 (2021).
21. L. Ortmann, A. S. Landsman, High-harmonic generation in solids. in *Advances in Atomic, Molecular, and Optical Physics* (Elsevier, 2021), pp. 103–156.
22. J. Alcalà, U. Bhattacharya, J. Biegert, M. Ciappina, U. Elu, T. Graß, P. T. Grochowski, M. Lewenstein, A. Palau, T. P. H. Sidiropoulos, T. Steinle, I. Tyulnev, High-harmonic spectroscopy of quantum phase transitions in a high-Tc superconductor. *Proc. Natl. Acad. Sci. U.S.A.* **119**, e2207766119 (2022).
23. A. Bharti, M. S. Mrudul, G. Dixit, High-harmonic spectroscopy of light-driven nonlinear anisotropic anomalous Hall effect in a Weyl semimetal. *Phys. Rev. B* **105**, 155140 (2022).
24. A. AlShafey, G. McCaul, Y.-M. Lu, X.-Y. Jia, S.-S. Gong, Z. Addison, D. I. Bondar, M. Randeria, A. S. Landsman, Ultrafast laser-driven dynamics in metal-insulator interface. *Phys. Rev B* **108**, 144434 (2023).
25. E. B. Molinero, A. Datta, M. J. Calderón, E. Bascones, R. E. F. Silva, High-harmonic generation with a twist: All-optical characterization of magic-angle twisted bilayer graphene. *Optica* **11**, 171–175 (2024).
26. T. Ikemachi, Y. Shinohara, T. Sato, J. Yumoto, M. Kuwata-Gonokami, K. L. Ishikawa, Time-dependent Hartree-Fock study of electron-hole interaction effects on high-order harmonic generation from periodic crystals. *Phys. Rev. A* **98**, 023415 (2018).
27. M. Udono, K. Sugimoto, T. Kaneko, Y. Ohta, Excitonic effects on high-harmonic generation in Mott insulators. *Phys. Rev. B* **105**, L241108 (2022).
28. Z. Nie, L. Guery, E. B. Molinero, P. Juergens, T. J. van den Hooven, Y. Wang, A. Jimenez Galan, P. C. M. Planken, R. E. F. Silva, P. M. Kraus, Following the nonthermal phase transition in niobium dioxide by time-resolved harmonic spectroscopy. *Phys. Rev. Lett.* **131**, 243201 (2023).
29. G. Vampa, B. G. Ghamsari, S. Siadat Mousavi, T. J. Hammond, A. Olivieri, E. Lisicka-Skrek, A. Yu Naumov, D. M. Villeneuve, A. Staudte, P. Berini, P. B. Corkum, Plasmon-enhanced high-harmonic generation from silicon. *Nat. Phys.* **13**, 659–662 (2017).
30. Z. Nourbakhsh, N. Tancogne-Dejean, H. Merdji, A. Rubio, High harmonics and isolated attosecond pulses from MgO. *Phys. Rev. Appl.* **15**, 014013 (2021).
31. F. Krausz, M. Ivanov, Attosecond physics. *Rev. Mod. Phys.* **81**, 163–234 (2009).
32. H. Haug, S. W. Koch, *Quantum Theory of the Optical and Electronic Properties of Semiconductors* (World Scientific Publishing Company, 2009).
33. G. L. Yudin, M. Y. Ivanov, Physics of correlated double ionization of atoms in intense laser fields: Quasistatic tunneling limit. *Phys. Rev. A* **63**, 033404 (2001).
34. T. Nubbemeyer, K. Gorling, A. Saenz, U. Eichmann, W. Sandner, Strong-field tunneling without ionization. *Phys. Rev. Lett.* **101**, 233001 (2008).
35. U. Eichmann, A. Saenz, S. Eilzer, T. Nubbemeyer, W. Sandner, Observing Rydberg atoms to survive intense laser fields. *Phys. Rev. Lett.* **110**, 203002 (2013).
36. U. Eichmann, S. Patchkovskii, "Frustrated tunneling ionization: Building a bridge between the internal and macroscopic states of an atom" in *Advances in Atomic, Molecular, and Optical Physics* (Elsevier, 2023), pp. 1–88.
37. R. R. Freeman, P. H. Bucksbaum, H. Milchberg, S. Darack, D. Schumacher, M. E. Geusic, Above-threshold ionization with subpicosecond laser pulses. *Phys. Rev. Lett.* **59**, 1092–1095 (1987).
38. M. V. Fedorov, A. M. Movsesian, Interference suppression of photoionization of Rydberg atoms in a strong electromagnetic field. *J. Opt. Soc. Am. B* **6**, 928 (1989).

39. M. V. Fedorov, M. Y. Ivanov, Coherence and interference in a Rydberg atom in a strong laser field: Excitation, ionization, and emission of light. *J. Opt. Soc. Am. B* **7**, 569 (1990).
40. M. V. Fedorov, N. P. Poluektov, A. M. Popov, O. V. Tikhonova, V. Y. Kharin, E. A. Volkova, Interference stabilization revisited. *IEEE J. Sel. Top. Quantum Electron.* **18**, 42–53 (2012).
41. M. P. de Boer, J. H. Hoogenraad, R. B. Vrijen, L. D. Noordam, H. G. Muller, Indications of high-intensity adiabatic stabilization in neon. *Phys. Rev. Lett.* **71**, 3263–3266 (1993).
42. M. P. de Boer, J. H. Hoogenraad, R. B. Vrijen, R. C. Constantinescu, L. D. Noordam, H. G. Muller, Adiabatic stabilization against photoionization: An experimental study. *Phys. Rev. A* **50**, 4085–4098 (1994).
43. M. Matthews, F. Morales, A. Patas, A. Lindinger, J. Gateau, N. Berti, S. Hermelin, J. Kasparian, M. Richter, T. Bredtmann, O. Smirnova, J. P. Wolf, M. Ivanov, Amplification of intense light fields by nearly free electrons. *Nat. Phys.* **14**, 695–700 (2018).
44. E. S. Toma, P. Antoine, A. de Bohan, H. G. Muller, Resonance-enhanced high-harmonic generation. *J. Phys. B.: At., Mol. Opt. Phys.* **32**, 5843–5852 (1999).
45. S. Beaulieu, S. Camp, D. Descamps, A. Comby, V. Wanie, S. Petit, F. Légaré, K. J. Schafer, M. B. Gaarde, F. Catoire, Y. Mairesse, Role of excited states in high-order harmonic generation. *Phys. Rev. Lett.* **117**, 203001 (2016).
46. N. Mayer, S. Beaulieu, Á. Jiménez-Galán, S. Patchkovskii, O. Kornilov, D. Descamps, S. Petit, O. Smirnova, Y. Mairesse, M. Y. Ivanov, Role of spin-orbit coupling in high-order harmonic generation revealed by supercycle Rydberg trajectories. *Phys. Rev. Lett.* **129**, 173202 (2022).
47. S. Beaulieu, E. Bloch, L. Barreau, A. Comby, D. Descamps, R. Géneaux, F. Légaré, S. Petit, Y. Mairesse, Phase-resolved two-dimensional spectroscopy of electronic wave packets by laser-induced XUV free induction decay. *Phys. Rev. A* **95**, 041401 (2017).
48. U. Bengs, S. Patchkovskii, M. Ivanov, N. Zhavoronkov, All-optical Stückelberg spectroscopy of strongly driven Rydberg states. *Phys. Rev. Res.* **4**, 023135 (2022).
49. J. Hader, J. Neuhaus, J. V. Moloney, S. W. Koch, Coulomb enhancement of high harmonic generation in monolayer transition metal dichalcogenides. *Opt. Lett.* **48**, 2094–2097 (2023).
50. K. Nagai, K. Uchida, S. Kusaba, T. Endo, Y. Miyata, K. Tanaka, Effect of incoherent electron-hole pairs on high harmonic generation in an atomically thin semiconductor. *Phys. Rev. Res.* **5**, 043130 (2023).
51. N. Yoshikawa, K. Nagai, K. Uchida, Y. Takaguchi, S. Sasaki, Y. Miyata, K. Tanaka, Interband resonant high-harmonic generation by valley polarized electron–hole pairs. *Nat. Commun.* **10**, 3709 (2019).
52. H. Liu, Y. Li, Y. S. You, S. Ghimire, T. F. Heinz, D. A. Reis, High-harmonic generation from an atomically thin semiconductor. *Nat. Phys.* **13**, 262–265 (2016).
53. Y. Kobayashi, C. Heide, A. C. Johnson, V. Tiwari, F. Liu, D. A. Reis, T. F. Heinz, S. Ghimire, Floquet engineering of strongly driven excitons in monolayer tungsten disulfide. *Nat. Phys.* **19**, 171–176 (2023).
54. R. Roldán, L. Chirolli, E. Prada, J. A. Silva-Guillén, P. San-Jose, F. Guinea, Theory of 2D crystals: Graphene and beyond. *Chem. Soc. Rev.* **46**, 4387–4399 (2017).
55. T. Galvani, F. Paleari, H. P. C. Miranda, A. Molina-Sánchez, L. Wirtz, S. Latil, H. Amara, F. Ducastelle, Excitons in boron nitride single layer. *Phys. Rev. B* **94**, 125303 (2016).
56. F. Ferreira, A. J. Chaves, N. M. R. Peres, R. M. Ribeiro, Excitons in hexagonal boron nitride single-layer: A new platform for polaritonics in the ultraviolet. *J. Opt. Soc. Am. B* **36**, 674 (2019).
57. W.-T. Hsu, J. Quan, C. Y. Wang, L. S. Lu, M. Campbell, W. H. Chang, L. J. Li, X. Li, C. K. Shih, Dielectric impact on exciton binding energy and quasiparticle bandgap in monolayer WS_2 and WSe_2. *2D Mater.* **6**, 025028 (2019).
58. H. T. Nguyen-Truong, Exciton binding energy and screening length in two-dimensional semiconductors. *Phys. Rev. B* **105**, L201407 (2022).
59. D. Guerci, M. Capone, M. Fabrizio, Exciton Mott transition revisited. *Phys. Rev. Mater.* **3**, 054605 (2019).
60. G. Vampa, C. R. McDonald, G. Orlando, D. D. Klug, P. B. Corkum, T. Brabec, Theoretical analysis of high-harmonic generation in solids. *Phys. Rev. Lett.* **113**, 073901 (2014).
61. E. Ridolfi, P. E. Trevisanutto, V. M. Pereira, Expeditious computation of nonlinear optical properties of arbitrary order with native electronic interactions in the time domain. *Phys. Rev. B* **102**, 245110 (2020).
62. G. Cistaro, M. Malakhov, J. J. Esteve-Paredes, A. J. Uría-Álvarez, R. E. F. Silva, F. Martin, J. J. Palacios, A. Picón, Theoretical approach for electron dynamics and ultrafast spectroscopy (EDUS). *J. Chem. Theory Comput.* **19**, 333–348 (2023).
63. J.-H. Choi, P. Cui, H. Lan, Z. Zhang, Linear scaling of the exciton binding energy versus the band gap of two-dimensional materials. *Phys. Rev. Lett.* **115**, 066403 (2015).
64. F. Zhang, C. S. Ong, J. W. Ruan, M. Wu, X. Q. Shi, Z. K. Tang, S. G. Louie, Intervalley excitonic hybridization, optical selection rules, and imperfect circular dichroism in monolayer *h*–BN. *Phys. Rev. Lett.* **128**, 047402 (2022).
65. A. Chernikov, T. C. Berkelbach, H. M. Hill, A. Rigosi, Y. Li, B. Aslan, D. R. Reichman, M. S. Hybertsen, T. F. Heinz, Exciton binding energy and nonhydrogenic Rydberg series in monolayer WS_2. *Phys. Rev. Lett.* **113**, 076802 (2014).
66. M. S. Mrudul, N. Tancogne-Dejean, A. Rubio, G. Dixit, High-harmonic generation from spin-polarised defects in solids. *NPJ Comput. Mater.* **6**, 10 (2020).
67. J. Sun, C.-W. Lee, A. Kononov, A. Schleife, C. A. Ullrich, Real-time exciton dynamics with time-dependent density-functional theory. *Phys. Rev. Lett.* **127**, 077401 (2021).
68. C. Kittel, *Introduction to Solid State Physics* (Wiley, ed. 8, 2004).
69. R. E. F. Silva, F. Martín, M. Ivanov, High harmonic generation in crystals using maximally localized Wannier functions. *Phys. Rev. B* **100**, 195201 (2019).
70. L. V. Keldysh, Coulomb interaction in thin semiconductor and semimetal films. *Sov. J. Exp. Theor. Phys. Lett.* **29**, 658 (1979).
71. P. Cudazzo, I. V. Tokatly, A. Rubio, Dielectric screening in two-dimensional insulators: Implications for excitonic and impurity states in graphane. *Phys. Rev. B* **84**, 085406 (2011).
72. A. H. Castro Neto, F. Guinea, N. M. R. Peres, K. S. Novoselov, A. K. Geim, The electronic properties of graphene. *Rev. Mod. Phys.* **81**, 109–162 (2009).
73. P. Giannozzi, S. Baroni, N. Bonini, M. Calandra, R. Car, C. Cavazzoni, D. Ceresoli, G. L. Chiarotti, M. Cococcioni, I. Dabo, A. Dal Corso, S. de Gironcoli, S. Fabris, G. Fratesi, R. Gebauer, U. Gerstmann, C. Gougoussis, A. Kokalj, M. Lazzeri, L. Martin-Samos, N. Marzari, F. Mauri, R. Mazzarello, S. Paolini, A. Pasquarello, L. Paulatto, C. Sbraccia, S. Scandolo, G. Sclauzero, A. P. Seitsonen, A. Smogunov, P. Umari, R. M. Wentzcovitch, QUANTUM ESPRESSO: A modular and open-source software project for quantum simulations of materials. *J. Phys. Condens. Matter* **21**, 395502 (2009).
74. A. A. Mostofi, J. R. Yates, Y.-S. Lee, I. Souza, D. Vanderbilt, N. Marzari, wannier90: A tool for obtaining maximally-localised Wannier functions. *Comput. Phys. Commun.* **178**, 685–699 (2008).

Acknowledgments

Funding: E.B.M. and R.E.F.S. acknowledge support from the fellowship LCF/BQ/PR21/11840008 from "La Caixa" Foundation (ID 100010434). This research was supported by grant PID2021-122769NB-I00 funded by MCIN/AEI/10.13039/501100011033. B.A. acknowledges support by Fundação para a Ciência e Tecnologia (FCT-Portugal) in the framework of the Strategic Funding UIDB/04650/2020, by project EXPL/FIS-MAC/0953/2021 and grant no. CEECIND/02936/2017. M.M. and A.P. acknowledge Comunidad de Madrid through TALENTO grant refs. 2017-T1/IND-5432 and 2021-5A/IND-20959 and the Spanish Ministry of Science, Innovation and Universities & the State Research Agency through grants refs. PID2021-126560NB-I00 and CNS2022-135803 (MCIU/AEI/FEDER, UE) and the "María de Maeztu" Programme for Units of Excellence in R&D (CEX2023-001316-M) and FASLIGHT network (RED2022-134391-T). **Author contributions:** E.B.M., B.A., M.I., P.S.-J., and R.E.F.S. developed the idea. E.B.M. performed the numerical calculations. M.M., G.C., and A.P. developed the numerical code used for the SBEs. E.B.M. developed the numerical code for the atomic TDSE. All authors contributed to analysis of the results. E.B.M., M.I., P.S.-J., and R.E.F.S. wrote the main part of the manuscript that was discussed by all authors. **Competing interests:** The authors declare that they have no competing interests. **Data and materials availability:** All data needed to evaluate the conclusions in the paper are present in the paper.

Submitted 22 December 2023
Accepted 29 July 2024
Published 30 August 2024
10.1126/sciadv.adn6985